RSC Advances

PAPER

View Article Online
View Journal | View Issue



Cite this: *RSC Adv.*, 2021, **11**, 24656

# Protection of lead-induced cytotoxicity using paramagnetic nickel–insulin quantum clusters†

Deepinder Sharda,[a] Komal Attri,[ab] Pawandeep Kaur[a] and Diptiman Choudhury *[ab]

Received 8th May 2021
Accepted 29th June 2021

DOI: 10.1039/d1ra03597e

rsc.li/rsc-advances

Pb-toxicity is associated with inflammation which leads to delay in wound healing. $Pb^{2+}$ utilizes calcium ion channels to enter the cell. Therefore, to achieve effective healing in a Pb-poisoned system, capturing $Pb^{2+}$ from the circulatory system would be an effective approach without hampering the activity of the calcium ion channel. In this work insulin–nickel fluorescent quantum clusters (INiQCs) have been synthesized and used for the specific detection of $Pb^{2+}$ ions *in vitro* and in cell-free systems. INiQCs (0.09 μM) can detect $Pb^{2+}$ concentrations as low as 10 pM effectively in a cell-free system using the fluorescence turn-off method. *In vitro* INiQCs (0.45 μM) can detect $Pb^{2+}$ concentrations as low as 1 μM. INiQCs also promote wound healing which can easily be monitored using the bright fluorescence of INiQCs. INiQCs also help to overcome the wound recovery inhibitory effect of $Pb^{2+}$ *in vitro* using lead nitrate. This work helps to generate effective biocompatible therapeutics for wound recovery in $Pb^{2+}$ poisoned individuals.



## 1. Introduction

Lead, a highly toxic, non-biodegradable element found ubiquitously in nature, causes environmental pollution, affects the human body to a large extent, and is among 275 most hazardous substances in the list of the Environmental Protection Agency (EPA), formulated by the Agency for Toxic Substances and Disease Registry (ATSDR).[1] Lead affects around 0.6% of the population globally[1] and causes acute and chronic toxicity even in minute quantities. Certain heavy metals, including $Pb^{2+}$, $Cd^{2+}$, and $Hg^{2+}$, can enter the body through food, water, smoking, industrial means, and even the skin surface, leading to heavy metal poisoning.[2,3] 600 ppm of lead is suggested as a "safe" level in the soil and would contribute under 5 μg $dL^{-1}$ to total blood lead of children below 12 years.[4] There is no relaxation in the maximum permissible limit for lead in water which was set at 0.05 ppm and is the highest desirable amount in drinking water in India. According to WHO, 1993, 25 μg $L^{-1}$ lead per kg body weight is the maximum tolerable amount weekly.[5] The daily exposure to $Pb^{2+}$ causes its deposition in body parts including liver, kidneys, spleen, and brain, causing multiple tissue damage by inducing oxidative stress. Moreover, long-term exposure to lead causes inflammatory infiltration, alterations in tissues of testicles, reduction in spermatocytes, necrosis of hepatocytes, degeneration of renal tubules, hypertrophy in the renal epithelium and induces endoplasmic reticulum stress due to calcium imbalance in the liver and kidney.[6,7] Kidneys are prone to the oxidative reaction of lead as lead intoxication sometimes causes dysfunctioning of proximal tubule or irreversible nephropathy depending on exposure regimens, thus adversely affecting the health of kidney function along with cadmium and mercury[8–10] and can be excreted through urine and feces.[11] It affects central nervous system causing several neurological disturbances affects the blood–brain barrier and causes edema and loss of neurons. The astroglial activation in the brain leads to pathological processes causing the death of neuronal cells, which causes the release of cytokines and chemokines, causing the inflammatory effect.[12] Also, children exposed to environmental lead are at a higher risk of toxicity because of absorption of ingested lead from the gastrointestinal tract and nervous system becoming more susceptible to neurotoxins.[13] $Pb^{2+}$ has a carcinogenic effect by damaging the DNA and disrupting its repair system by generating ROS (reactive oxygen species). It can even impair memory and learning in the brain by disrupting NMDAR (*N*-methyl-D-aspartate receptors).[14] Lead causes damage to epithelial tissues causes rashes and get accumulated over the epidermal surface.[15,16] Lead toxicity is dosage-dependent and include cellular traction forces, mechanical stiffness, focal adhesions, the shape of the cell, speed of migration, permeability, and wound healing efficacy in mammalian cells.[17–19]

At the molecular level, lead affects the humoral and cellular immune responses through various inflammatory biomarkers[20] including cytokines (IL-8, TNF, *etc.*), acute phase proteins including CRP, haptoglobin, and ceruloplasmin, enzymes involved in inflammation such as COX-2 and damages

[a]*School of Chemistry and Biochemistry, Thapar Institute of Engineering and Technology, Patiala, 147004, Punjab, India. E-mail: diptiman@thapar.edu; Tel: +91-8196949843*

[b]*Thapar Institute of Engineering and Technology-Virginia Tech (USA) Center of Excellence in Emerging Materials, Thapar Institute of Engineering and Technology, Patiala, Punjab-147004, India*

† Electronic supplementary information (ESI) available. See DOI: 10.1039/d1ra03597e

intracellular molecules mediators and decreases immunoglobulin production, making individuals more prone to inflammation and other diseases.[1,21]

To cope up with the toxic lead and its accumulation in the body the quantum clusters are being used as one of the efficient ways for its detection up to a picomolar level in a cell-free system and can be detected well *in vitro*.[22,23] For this purpose, insulin nickel quantum clusters were prepared as nickel metal plays a role in cell growth and wound healing activities.[24] Further, nickel is also a micronutrient essential for the proper functioning of the human body, as it increases hormonal activity and is involved in lipid metabolism. Nickel deficiency in mice resulted in a significant decrease in the activity of lipogenic enzymes, including glucose-6-phosphate dehydrogenase, 6-phosphogluconate dehydrogenase, malic enzyme, and fatty acid synthase deficiency.[25,26]

At present, QCs are preferred, as they emit luminescence because of high photostability, high emission rates, large stokes shift.[27–29] They act as a bridge between the nanoparticles, atoms, and bulk molecules and due to their size up to fermi wavelength affect optical, chemical, and electronic properties to a large extent based on different sizes.[30,31] QCs have few particles in the core as compared to the surface and are highly stable due to the presence of ligands with which surface atoms bind.[32] Different noble metals including gold, silver, copper, and zinc were used to make water-soluble QCs using mild reductants including glutathione, alkyl thiol, and $NaBH_4$ along with different peptides, proteins, amino acids, dendrimers, and DNA which can be used as templates.[33–35] A variety of protein, including proteins such as lactotransferrin, hemoglobin, BSA has been used for making QCs with $Au^+$, $Fe^{2+}$, $Cu^{2+}$, $Ca^{2+}$, $Ag^+$ (ref. 36–38) which exhibited optical properties, catalytic activity, and fluorescence thus, can be used in bio-imaging, natural marking, bio detecting of proteins, nucleic acids, and enzymes, and biological changes linked to them after translation or transcription.[39–42]

Insulin is widely used nowadays because the receptors for insulin are present on the membrane of all mammalian cells and their number greatly varies from 40 for erythrocytes to 200–$300 \times 10^3$ for adipocytes and hepatocytes. The insulin receptors are much higher in number in cancerous cells as compared to normal cells.[43–45] The insulin protein acts as a growth factor which facilitates chemotaxis and pinocytosis or phagocytosis by macrophages and promotes secretion of inflammatory mediators and helps in re-epithelialization which is crucial for healing wounds.[46] Different QCs using insulin as protein template is with silver as a drug carrier, gold which was used for super-resolution microscopy, copper for bioimaging applications, and zinc for wound healing.[47–49]

Here insulin-nickel fluorescent quantum clusters have been made, and it's been used for sensing of $Pb^{2+}$ sensing in a cell-free system and countering of it's poising and *in vitro*.

# 2. Materials and methods

## 2.1. Materials

All the metal salts of analytical grade, including $NiSO_4$ (nickel sulphate) and $Pb(NO_3)_2$ (lead nitrate) were purchased from Loba Chemie, India. Recombinant human insulin was purchased from (Elli Lilly, India). DMEM cell culture media, fetal bovine serum (FBS), penicillin–streptomycin were purchased from HiMedia, India. The rest of the chemicals were purchased from HiMedia and were of analytical grade.

## 2.2. Preparation of insulin quantum clusters with nickel metal salt

The metal salt was converted into insulin protected quantum clusters by following the standard protocol. The final concentration of both insulin and $NiSO_4$ was made at 1.82 μM in an aqueous medium. NaOH was used to adjust the insulin pH up to 10.5. This is labeled as solution A and kept in the dark. After this, salt solutions having molarity of 1.82 μM ($NiSO_4$) were prepared in a covered glass vial and labeled as solution B. Thereafter, solution A and B were mixed, and pH was adjusted by using HCl (0.1 N) at 7.4. The resulting solution was kept for incubation for 48 h at 37 °C at slow stirring (240 rpm).[50–52]

## 2.3. Spectroscopic characterization of INiQCs

**2.3.1. UV-visible spectroscopy.** UV-visible absorbance of INiQCs was measured using instrument UV-2600 spectrophotometer Shimadzu and 4000 μl quartz cuvette with 1 cm path and operated in the range 200 nm to 800 nm. The absorption spectra for insulin, salt solution ($NiSO_4$), and insulin linked nickel-metal quantum clusters (INiQCs) were measured to find out the interactions between insulin protein and $NiSO_4$ metal salt solution.

**2.3.2. Fluorescence spectroscopy.** Fluorescence data of insulin metal quantum clusters was measured using Agilent technologies Cary Eclipse fluorescence spectrophotometer. It helps determine insulin binding to the metal salt solutions to form fluorescent protein-linked metal quantum clusters. It was done for INiQCs, insulin, and $NiSO_4$ solution, all having similar concentrations. The fluorescence intensity was measured at an excitation wavelength of 272 nm, coupled with an emission scan from 280 nm to 800 nm with an excitation and emission slit of 20 mm.

Along with this heavy metal sensing experiment was also performed using the following protocol. 1 mM solution of $Pb^{2+}$ metal ion was made using nitrates of the salt. The solution thereafter undergoes 10 folds of 1/10th dilution. 1800 μl of the sample was taken from each solution obtained in the above dilution series, and 200 μl of INiQCs were added to each solution. The luminescence is measured immediately after the addition of the heavy metal ions into quantum clusters. The data obtained were analyzed to check out any quenching due to heavy metal ions in fluorescence. Also, a 1 mM solution of other heavy metals and certain cationic and anionic species were made using the above-described method. As a result, a dilution series was obtained for each of the ions, including $Cd^{2+}$, $Cu^{2+}$, $Hg^{2+}$, $Zn^{2+}$, $Ca^{2+}$, $K^+$, $Na^+$, $Cl^-$, $OH^-$, $HCO_3^-$, $SO_4^{2-}$, $S^{2-}$. For each sample, 1800 μl of the solution of the above-mentioned ions, 200 μl of INiQCs having pH 10 were added followed by instant measurement of fluorescence intensity to find out the specificity.

The percentage increase in intrinsic fluorescence intensity was calculated and compared for both insulin and INiQCs using the given eqn (1)

$$\%\ \text{of change in emission intensity} = \frac{\text{F.I.(INiQCs)} - \text{F.I.(insulin)} \times 100\%}{\text{F.I.(insulin)}} \quad (1)$$

A similar formula was used to find out the % change in emission intensity after adding $Pb^{2+}$ metal ions into INiQCs. For finding out the quantum yield of both insulin and insulin protected quantum clusters of nickel (INiQCs), the standard tyrosine fluorescence quantum yield was used as in eqn (2)

$$\text{Q.Y.}(S) = \frac{\text{Q.Y.(Tyr)} \times I(S) \times 1 - 10^{-Al}(\text{Tyr}) \times n^2(S)}{\text{I(Tyr)} \times 1 - 10^{-Al}(S) \times n^2(\text{Tyr})} \quad (2)$$

here, Q.Y.is quantum yield; $I$ is integrated emission intensity; $n$ is refractive index of solvent; $A$ is the absorbance at excitation wavelength; $l$ is the length of absorption cell; Tyr is tyrosine (reference) and $S$ is sample.

**2.3.3. FTIR analysis to determine variation in wavenumber after QCs formation.** Agilent Cary 600 series FTIR Spectrophotometer was used to find out the functional groups present in the above-mentioned INiQCs and insulin. The samples after washing were air-dried on a glass side at 37 °C before using them. Then the pellets were mixed with potassium bromide (KBr), and scanning was done from 400 $cm^{-1}$ to 4000 $cm^{-1}$.

**2.3.4. Morphological and elemental analysis using DLS and HRTEM.** We have performed DLS (dynamic light scattering) to find out the hydrodynamic size of INiQCs formed using a Malvern DLS-Zeta size analyzer. Thereafter, to find out the morphology of insulin linked nickel quantum clusters High-Resolution Transmission Electron Microscopy (HRTEM) Talos F200S G2, Thermo Scientifics, and Selected Area Electron Diffraction (SAED) was used. For this, the samples were centrifuged at 240 rpm for nearly 10–15 minutes, followed by a thorough washing of the pellet to eliminate unbound metal salt or impurities associated with the sample.

In addition to HRTEM, Electron Dynamic Scattering (EDS) was performed in which the same pellet was investigated to get the percentage of elemental constituents present in the sample.

**2.3.5. Stoichiometry ratio of $Ni^{2+}$ ions: insulin protein.** The stoichiometry of nickel ions to insulin protein are calculated using the following equation to find out the interactions taking place between ligand that is metal ion and complex protein

$$\text{Number of proteins bound to single } Ni^{2+} \text{ ion} = \frac{\text{average number of bound proteins per ml}}{\text{average number of } Ni^{2+} \text{ ions per ml}} \quad (3)$$

Further, for calculating the stoichiometry of INiQCs to $Pb^{2+}$ ions present we have done job's plot by keeping the total concentration constant and varying the individual concentration of ligand and complex.

### 2.4. *In silico* studies to determine interactions between nickel-metal and insulin protein

To find out the binding site residues of different transition metal ions with the help of the fragment transformation method, an online docking server tool that is MIB (Metal Ion Binding) can be used. To apply this method, two different protein chains were required, which were extracted from the protein data bank (PDB) and consist of the template protein (T) of length $m$ containing metal-ion and query protein (S) of length $n$. These chains were then aligned such that after proper alignment, the metal ion binding protein template can be converted into the query protein structure. To get these protein structures, certain different parameters were followed. Firstly, the most important parameter is that the metal ion template must contain residues bound with transition metals, including $Ni^{2+}$, $Cu^{2+}$, $Mg^{2+}$, $Ca^{2+}$, $Co^{2+}$, $Zn^{2+}$, $Fe^{2+}$, and $Fe^{3+}$ metal ions. Secondly, the polypeptide chain length in protein structures must be 50 residues; otherwise, it will be excluded.[53] The residues of query template and metal ion binding triplets can be written by using the notation N–Cα–C backbone atoms and as ($x$N, $x$Cα, $x$C) and ($y$N, $y$Cα, $y$C); where $x$ and $y$ are PDB coordinates. S and T can be written as (τ1, τ2…τ$m$) and (σ1, σ2…σ$m$) in terms of triplets. The third parameter is, there should be at least two metal ion binding residues, and the distance in between the PDB coordinates and metal center should be within 3.5 Å. Proper alignment is possible only if the distance is less than 3.5 Å.[54] The fourth most important parameter is that the residue's binding score should be more than a specified threshold value, and only then will residue bind to particular transition metal ions. The binding score is denoted by Ci, and based on the sequence of target protein along with structural conservation of protein; the binding score is assigned to all the residues of the target protein by using root mean square deviation of C-alpha carbons of structural local alignment as well as BLOSUM62 substitution matrix.[55,56] Hence, the binding site of metal ions was determined using the bioinformatics tool.

In this way, the MIB tool helps determine the binding site of metal ions on a particular protein chain. Human insulin protein (PDB ID: 4EWW) was extracted from the PDB (Protein Data Bank) database. This polypeptide contains 2 chains denoted by A and B. In the MIB tool, $Ni^{2+}$ metal ion was docked with chains A and B of human insulin independently, followed by comparing metal ion-binding templates with the target protein.[57]

### 2.5. Cytotoxicity testing using QCs prepared

To check out the viability of cells HEK 293 cell line (Human Embryonic Kidney Cells) was used and MTT (3-(4,5-dimethylthiazol-2-yl)-2,5-diphenyltetrazolium bromide) the assay was performed. For this purpose, HEK 293, having a density of $1 \times 10^4$ (per well density), has been seeded in 96 well plates and was allowed to become confluent up to 70–75%. After this incubation of cells using 3 different percentages (1.5, 7.5, and 30 μM) of INiQCs, insulin, $NiSO_4$, and a mixture of insulin and $NiSO_4$ was done. Following this treatment, cells were incubated in an incubator for 24 h and 37 °C. After 24 h,

the MTT (2 mg $mL^{-1}$ in 5% ethanol) was added and kept as such for 3 h. After 3 h MTT and media were both removed from every well of 96 well plates, followed by the addition of 200 μl dimethyl sulfoxide (DMSO) to dissolve the formazan crystals, and then the absorbance was checked at 570 nm. To calculate the inhibition percentage following equation was used.

$$\% \text{ inhibition} = [1 - (A_t/A_c) \times 100]\% \quad (4)$$

where $A_t$ is the test substance absorbance and $A_c$ control solvent absorbance. For each of the concentrations.[58]

Following this, another MTT was performed. In this, we add 6 different concentrations (0, 1, 10, 100, 500, 1000 μM) of $Pb^{2+}$ in each of the initially incubated cell lines with INiQCs, insulin, $NiSO_4$, and a mixture of insulin and $NiSO_4$ as described above. After incubation for 12 h, the MTT was added, and all the steps were followed as above.

While performing MTT assay, both in presence and absence of heavy metal $Pb^{2+}$, three independent replicate sets were taken for each concentration. Then an average of all those readings was calculated and plotted along with the error bars based on standard deviation.

### 2.6. Fluorescence imaging to determine role of INiQCs in bio-imaging

Fluorescence imaging was done using the Dewinter fluorescence microscope. For doing bioimaging, by using UV light in UV-laminar, the samples were incubated for one h. Then, 100 μl from the insulin metal quantum clusters (INiQCs) was taken and added to the cell line opted for the experiment that is human embryonic kidney cell line (HEK 293). Thereafter, to remove any impurities, samples were washed with PBS buffer twice, and cells were fixed by adding 2% of formaldehyde solution. Then, in coverslip covered 6 well plates, HEK 293 cell lines with the added quantum clusters were kept for incubation for 1 day. Later on, a fluorescence microscope was used for having images of the incubated cells with and without using a magnet.

Similarly, in the other 6 well plates, the above samples were again made as such, followed by the addition of 6 different concentrations (0, 1, 10, 100, 500, 1000 μM) of $Pb^{2+}$ in each of the initially incubated well to find out the variation in fluorescence emission intensity *in vitro*. Thereafter, bioimaging was done using a microscope.

### 2.7. Effect of INiQCs on recovery of wound in presence of toxic element $Pb^{2+}$ using phase contrast and fluorescence imaging

The cells were cultured in 60 mm plates using the high glucose DMEM-F12 FBS-free medium. The cells were incubated at 37 °C and 5% $CO_2$. The cells were allowed to grow and be 80–85% confluent. Thereafter, the cell scratch method was used for making a wound, and the cells were treated with different concentrations of INiQCs, insulin, Ni salt, and the mixture of insulin and Ni salt (I + Ni). In one more plate, cells were treated initially with lead, followed by treatment with INiQCs. Time-lapse imaging was done, and the variation in the width of the wound was measured after 6 h, 12 h, and 24 h, respectively. We measure wound width at different positions randomly for each scratch-made in the individual well plate and took the mean of those independent readings of wound diameter to calculate percentage change in wound diameter.

## 3. Results and discussions

### 3.1. Absorbance spectra to determine variation in absorbance after INiQCs formation

After the synthesis of INiQCs, its characterization was done. We obtained a sharp peak for insulin without any added metal salts at 272.03 with an absorbance value of 0.249, whereas on the other hand, after incubating the insulin with metal salts for 48 h, an absorbance value of 0.135 was obtained for quantum clusters having a peak at 272 nm Fig. 1a. This confirms the synthesis of INiQCs. The absorption peak is also compared with that of a tyrosine as it was selected as a standard, Fig. S1a.†

### 3.2. Fluorescence spectra to measure fluorescence intensity of INiQCs formed

For INiQCs, at an excitation wavelength of 270 nm, an emission peak ranging from 280–360 nm was obtained with maxima at ~300 nm with the intensity of 240.52 a.u. When it was monitored from 200–800 nm, as shown in Fig. 1b.

To determine the quantum yield of INiQCs, tyrosine was used as a standard as its quantum yield value is known. The % change in fluorescence was calculated. In comparison to insulin, the percentage change for INiQCs is 48.26%, but when adding $Pb^{2+}$ ions (10 pM) into INiQCs, the value decreases to 26.5%. The quantum yield of insulin was found out to be 0.1798, and that of INiQCs turned out to be 0.7416. After adding $Pb^{2+}$ into INiQCs, the quantum yield obtained was 0.4626 (Fig. S1b†).

For the metal salts, it has been observed that when we add insulin to the salt solution, the intensity of the emission peak increases.

### 3.3. Structure, composition and stoichiometry of metal insulin clusters

The hydrodynamic size of INiQCs was found out to be 1400 ± 150 nm (Fig. S1c†). For the stability of complex in buffer, we have done DLS measurements in PBS buffer on day 1 and after 6 months (day 196). The hydrodynamic size in buffer was found to be 1350 ± 150 nm which is quite in similar to the one done earlier 1400 ± 150 nm (on day 1), thus the results indicating the stability of the formulation in 1× PBS in buffer (when stored at 4 °C). The hydrodynamic diameter values samples in DMEM media without fetal bovine serum was checked at different time points and was found 1300 ± 200 nm, 1350 ± 200 nm, and 2000 ± 200 nm for 6 h, 12 h and 24 h incubation respectively at 37 °C, which indicates there is an interaction between INiQCs and media components. The spherical quantum clusters of INiQCs were formed and confirmed by Transmission electron microscopic images. All the quantum clusters are distributed over the

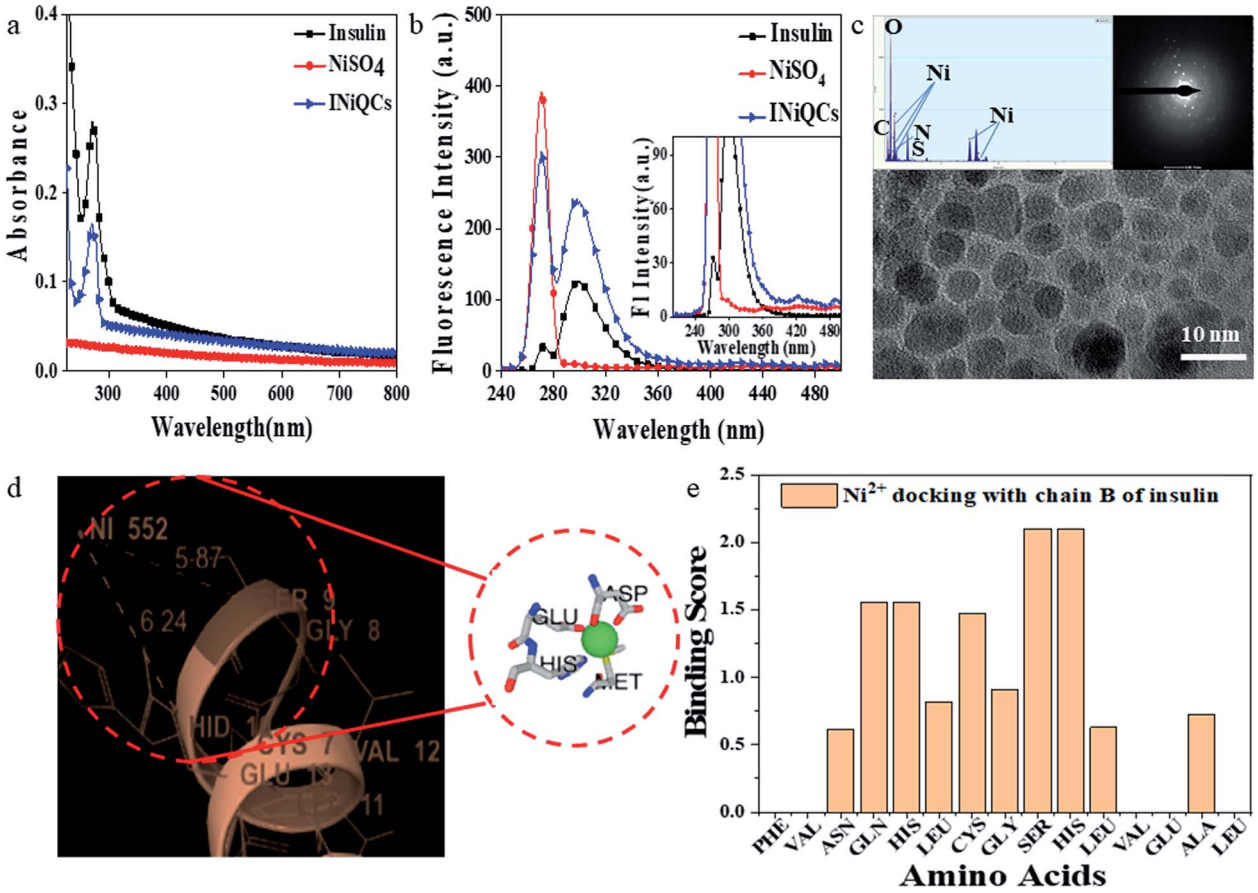


Fig. 1 Characterization of INiQCs (a) the excitation peak of insulin was shown at 272 in absorption spectra and after incubation with $NiSO_4$, maxima at 272 nm is obtained for INiQCs in absorption spectra. (b) Shows the fluorescence spectra after excitation of controls (insulin, and $NiSO_4$) and INiQCs at a wavelength of 272 nm, and an emission spectrum is obtained which exhibits maximum fluorescence intensity at 299.36 nm when scanned from 200–800 nm. Inset is the trailing of fluorescence from 380 nm onwards. (c) HRTEM images on a 10 nm scale showing the ~5–6 nm size of INiQCs, inset is the HRTEM-EDS showing that the Ni is present in the quantum clusters along with the selected area electron diffraction (SAED) confirming the presence of Ni in the INiQCs. (d) Metal ion binding residues: depicts the binding site for $Ni^{2+}$ with the amino acid residues within 3.55 Å diameter that can participate in binding on chain B of insulin (e) binding potential of each amino acid with the $Ni^{2+}$ ion.

protein matrix in small clusters. As shown by High-Resolution Transmission electron microscopic images (HRTEM), the size of clusters is ~5–6 nm. The presence of a significant amount of Ni in quantum clusters is indicated by HRTEM-EDS images and confirmed by the diffraction pattern. The SAED (selected area electron diffraction) pattern is attached at the top, which shows a ring-like pattern in Fig. 1c. The presence of different elements like Ni, C, O, N, and S is shown in the elemental mapping of the area. The even distribution and percentage of Ni associated with protein come out to be 5.28% and analyzed by EDS (inset of Fig. 1c). Further, the stoichiometric ratio between insulin protein and $Ni^{2+}$ ions were calculated and found that one $Ni^{2+}$ ion (163 pm in radius) is encapsulated by ~687 insulin protein.

### 3.4. *In silico* studies using metal-ion binding residue templates for nickel and insulin interaction

We used MIB (Metal Ion Binding), which is an online docking server. With the help of this tool, we were able to find the binding sites of insulin with which transition metal $Ni^{2+}$ can bind. The interaction of the protein with metals is largely based on the amino acids' structure and sequence in a protein. Firstly, the sequence of human insulin was extracted from the Protein Data Base (PDB ID: 4EWW) and then inserted in the MIB (Metal Ion Binding) tool to dock the $Ni^{2+}$ ions with both the chains (chain A & B) of insulin. As a result, a binding score was assigned to each residue in the insulin protein. If the binding score was more than the threshold, that particular residue is considered the binding site for that particular metal ion. Therefore, the binding sites for metal ions $Ni^{2+}$ were determined. The data indicates that chain A does not show any template indicating the absence of binding sites of $Ni^{2+}$ ions with chain A whereas in chain B, a binding site was found for $Ni^{2+}$ ions. Then we worked with another software called Maestro. Using this, we calculated the distance between the metal ion and its binding site, that is, amino acids, namely 9 SER and 10 HIS present on Chain B of insulin. The distance was found out to be 5.87 and 6.24, respectively, as shown in Fig. 1d. The binding score was also determined using MIB with

different amino acids present in chain B of insulin with $Ni^{2+}$ ions, thus finding the best possible sites for attachment (Fig. 1e). The binding of nickel ions with different amino acids is determined through different orientations of the metal-binding amino acids in proteins, as shown in Fig. S2a–d.† The binding score of different amino acids with nickel ions is shown in Table S1.†

### 3.5. FTIR analysis for studying the interaction between nickel and insulin

To figure out the interactions involved in metal–protein binding, FTIR was used for $NiSO_4$, insulin, and INiQCs. The peaks appeared due to intermolecular interactions of insulin and $NiSO_4$ at different wavenumbers. Firstly, the peak appeared at 670 $cm^{-1}$ which indicates the Ni–OH bending bond formation.[59] Then a peak at 742 $cm^{-1}$ was observed both in insulin and INiQCs, indicating $NH_2$ and NH wagging.[36] In addition to the first peak, a peak at 820 $cm^{-1}$ shows the bond between Ni=O confirms the interaction in insulin and $NiSO_4$.[60] A peak at 881 $cm^{-1}$ in insulin shows C–O stretching. C–N stretching was observed both in insulin and INiQCs at 1046 $cm^{-1}$. Multiple S=O stretching peaks were observed, firstly at 1198 $cm^{-1}$ in INiQCs and $NiSO_4$, followed by a peak at 1288 $cm^{-1}$ both in insulin and $NiSO_4$ and finally at 1415 $cm^{-1}$ in INiQCs and $NiSO_4$.[49] C–H bond was observed in insulin at 1388.5 $cm^{-1}$.[61] Amide II is the $NH_2$ bond was seen in insulin at 1528 $cm^{-1}$ and 1590 $cm^{-1}$ but only at 1590 $cm^{-1}$ in INiQCs.[62] C–H stretching was observed at 2869.7 $cm^{-1}$ in insulin only.[53] Intramolecular O–H stretching gives two peaks in INiQCs at 2958 $cm^{-1}$ and 3187.6 $cm^{-1}$ respectively, but a single peak was observed at 3187.6 $cm^{-1}$ in $NiSO_4$.[63] A single peak was there in insulin, indicating amine N–H stretching at 3330 $cm^{-1}$ which was absent in the other two.[49] For non-H-bonded O–H stretching peaks were observed at 3682 $cm^{-1}$ and 3782.5 $cm^{-1}$ both in INiQCs and $NiSO_4$ but were absent in insulin.[59] This is shown in Fig. S3a† and Table 1.

### 3.6. Heavy metal ($Pb^{2+}$) detection by luminescence quenching in cell-free system

The luminescence of INiQCs can be used as a highly selective and sensitive tool to detect $Pb^{2+}$ ions by a "turn-off" luminescent sensor. Fluorescence quenching is observed in the presence of $Pb^{2+}$ ions, and it greatly varies with the concentration of $Pb^{2+}$ ions Fig. 2a. The greater the concentration of heavy metal ion, the more will be quenching, and the less will be the fluorescence intensity as shown in the inset of Fig. 2a. Fluorescence quenching was maximum when the concentration of $Pb^{2+}$ ions was maximum, 10 millimolar in this case, and declines gradually as concentration reaches up to 10 picomolar levels. Various other metal ions were also used to find out if fluorescence due to INiQCs decreases or increases in their presence, but no such effect was found for $Cd^{2+}$, $Hg^{2+}$, $Cu^{2+}$, $Zn^{2+}$, $Ca^{2+}$, $K^{+}$, $Na^{+}$, $Cl^{-}$, $OH^{-}$, $HCO_3^{-}$, $S^{2-}$, $SO_4^{2-}$ when we use their highest concentration similar to that of lead ions, that is 10 mM. Fluorescence was immediately measured after adding the QCs into the salt solutions of the highest concentration. However, no such effect was observed with any of the other metal ions Fig. 2b. Then the variation in fluorescence intensity of insulin, INiQCs, $NiSO_4$, tyrosine, INiQCs + $Pb^{2+}$ was measured to compare the differences between all and calculate quantum yield, which comes out to be 0.7416 for INiQCs and 0.4626 when we add the $Pb^{2+}$ ions Fig. 2c. Further, the stoichiometric ratio was calculated using the job's plot for INiQCs and $Pb^{2+}$ and found to be 1 : 1, as shown in Fig. 2d.

### 3.7. HEK 293 cell viability and migration assay

The MTT result for cell viability is highly dependent on the mitochondrial activity of cells. It is calculated for insulin, $NiSO_4$, a mixture of insulin and $NiSO_4$ and INiQCs by using 1.5, 7.5, and 30 μM of concentrations and the graph were plotted. While performing MTT assay, both in the presence and absence

Table 1 The comparative wavenumber values of insulin, $NiSO_4$ and INiQCs showing the position of different functional groups present which coins the interaction amongst insulin and $NiSO_4$ salt solution

| Functional groups | Insulin | $NiSO_4$ | INiQCs | Reference number |
|---|---|---|---|---|
| Ni–OH bonding | — | — | 670 | 59 |
| $NH_2$ and NH wagging | 742 | — | 742 | 36 |
| Ni=O stretching | — | — | 820 | 60 |
| C–O stretching | 881 | — | — | 49 |
| C–N stretching | 1046 | — | 1046 | 49 |
| S=O stretching | — | 1198 | 1198 | 49 |
| | 1288 | 1288 | — | |
| | — | 1415 | 1415 | |
| C–H bond | 1388.5 | — | — | 61 |
| Amide C=O bond | 1528 | — | — | 62 |
| | 1590 | — | 1590 | |
| C–H stretching vibrations | 2869.7 | — | — | 53 |
| O–H intermolecular stretching | — | — | 2958 | 63 |
| | — | 3187.6 | 3187.6 | |
| Amine N–H stretching | 3330 | — | — | 49 |
| O–H stretching (non-H bonded) | — | 3682 | 3682 | 59 |
| | — | 3782.5 | 3782.5 | |

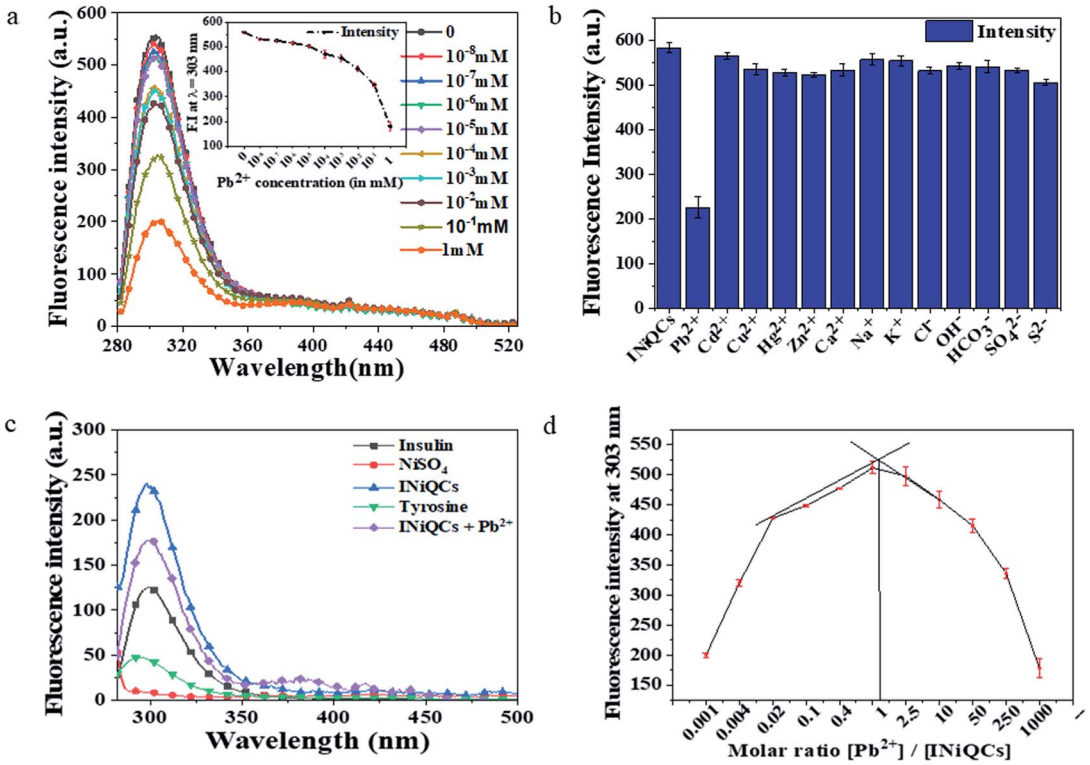


Fig. 2 Sensing of $Pb^{2+}$ in a cell-free system using INiQCs. (a) Shows the variation in fluorescence spectra after excitation of all samples at 272 nm. An emission-spectra was obtained, showing a gradual decrease in fluorescence with increasing concentration of $Pb^{2+}$ ions from $10^{-8}$ mM of $Pb^{2+}$ to 0 mM of $Pb^{2+}$. Inset is the decrease in fluorescence intensity at $\lambda_{max}$ with varying concentrations of $Pb(NO_3)_2$. (b) Variation in fluorescence intensity at $\lambda_{max}$ for different metal ions, including heavy metal ions and other cations and anions. (c) It shows the fluorescence spectra of INiQCs, INiQCs + $Pb^{2+}$, insulin, $NiSO_4$, and tyrosine, indicating variation in fluorescence intensity. (d) It shows job's plot for the determination of stoichiometry between INiQCs and $Pb^{2+}$ ions. *X*-axis represents the molar ratio between INiQCs and $Pb^{2+}$.

of heavy metal $Pb^{2+}$, three independent replicate sets were taken for each concentration. Then an average of all those readings were calculated and plotted along with the error bars based on standard deviation. For $NiSO_4$ treated cells, cell viability shown is 102.94 ± 3.20% for 1.5 μM, 125.16 ± 1.27% for 7.5 μM and 131.35 ± 10.96% for 30 μM. Insulin shows 113.1 ± 4.60% for 1.5 μM, 129.76 ± 0.49% for 7.5 μM and 157.41 ± 18.47% for 30 μM, respectively. The cells exposed to a combination of insulin and $NiSO_4$ showed more cell viability. It is 141.03 ± 3.03% for 1.5 μM, 151.98 ± 2.46% for 7.5 μM and 162.3 ± 9.32% for 30 μM respectively. Cell division after treatment with INiQCs showed much more significant changes, which are 139.29 ± 1.13% for 1.5 μM, 189.68 ± 1.64% for 7.5 μM, and 195.63 ± 7.36% for 30 μM respectively as compared with treated and untreated controls. The results suggested that these quantum clusters have the potential to enhance cell division and can help in wound healing. The measurements were statistically significant. From the graph, it was demonstrated that no one is toxic in comparison to the control. With increasing the concentration of samples added, the cell viability enhanced and was maximum for INiQCs formed indicating that quantum clusters formed are not at all toxic instead, they help in the cell division, and multiplication thus can be used for wound healing, as well as shown in Fig. 3a and S4a.†

Similarly, when we add different concentrations of $Pb^{2+}$ ranging from 0, 1, 10, 100, 500, 1000 μM respectively in the cells initially incubated with insulin, $NiSO_4$, a mixture of insulin and $NiSO_4$ and INiQCs, the MTT results show that the cell growth declined gradually with increasing concentration of lead metal ions in all the wells, but in the presence of INiQCs, the cell growth is less impaired. The cell viability is calculated for all the samples. For cells incubated only with $Pb^{2+}$ the cell viability is 97.71 ± 4.46% for 1 μM, 98.07 ± 1.85% for 10 μM, 43.31 ± 17.26% for 100 μM, 41.64 ± 5.11% for 500 μM and 28.84 ± 0.92% for 1000 μM. When we add the above-mentioned concentrations of $Pb^{2+}$ with a fixed concentration of $NiSO_4$ the cell viability comes out to be 100.84 ± 2.17% for 1 μM, 103.31 ± 3.84% for 10 μM, 61.58 ± 8.05% for 100 μM, 65.43 ± 0.65% for 500 μM and 46.49 ± 7.62% for 1000 μM. A fixed concentration of insulin shows 107.15 ± 1.34% for 1 μM, 100.53 ± 6.36% for 10 μM, 79.59 ± 12.47% for 100 μM, 50.03 ± 10.36% for 500 μM and 27.40 ± 7.97% for 1000 μM. The cells incubated with a mixture of insulin and $NiSO_4$ have cell viability as 92.76 ± 4.02% for 1 μM, 91.30 ± 3.86% for 10 μM, 49.88 ± 7.40% for 100 μM, 46.80 ± 7.40% for 500 μM, and 25.71 ± 2.54% for 1000 μM. The cells exposed to INiQCS have the maximum cell viability out of all these, even in the presence of a varying concentration of $Pb^{2+}$ which is 103.38 ± 5.55% for 1 μM, 104.92 ± 1.63% for 10 μM, 79.95 ± 8.66% for 100 μM, 80.16 ± 6.53% for 500 μM and 61.63

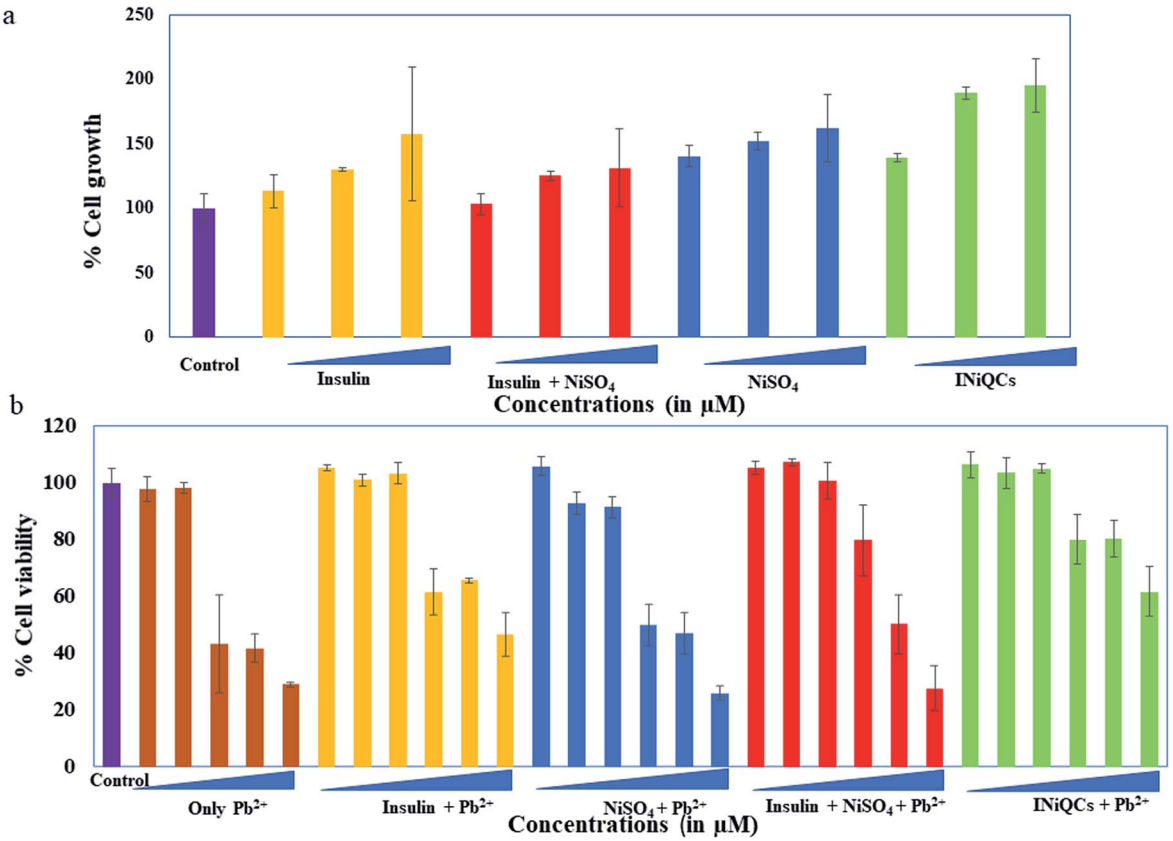


Fig. 3 MTT assay to determine the growth rate of cells. (a) Data shows treatment of HEK-293 cells with control including insulin, $NiSO_4$, insulin + $NiSO_4$, and INiQCs ranging from 1.5, 7.5, and 30 μM concentration respectively of each sample. (b) Data shows treatment of HEK-293 cells with 0.45 μM of insulin, $NiSO_4$, insulin + $NiSO_4$, and INiQCs. Then the same cells were treated with 0, 1, 10, 100, 500, 1000 (μM) concentration of $Pb^{2+}$ after 3 h and data were plotted as the mean value of three independent experiments.

± 8.86% for 1000 μM. The cells keep on growing without much effect of heavy metal ion even in the highest concentrations of $Pb^{2+}$ ion which are 100, 500, and 1000 μM respectively. This indicates that INiQCs are not toxic themselves, overcome the effect of toxicity due to $Pb^{2+}$, and further results in improving cell multiplication and growth as shown in Fig. 3b and S4b.†

INiQCs induced more cell migration as compared to untreated and treated controls including $NiSO_4$, insulin, insulin + $NiSO_4$. With the increasing time, the extent of cell division and migration increased at a fixed concentration that is 0.45 μM. For the measurement of change in wound diameter, we measure wound width at six distinguished positions for each scratch made in an individual well plate and took the mean of those independent readings of wound diameter to calculate percentage change in wound diameter. The cells treated with INiQCs shows the percentage of a gap left between the scratched wound after 6, 12, and 24 h as 40.90 ± 4.54%, 27.62 ± 5.99%, and 8.51 ± 2.83% Fig. 4(m–o and r–t) respectively in comparison to untreated control scratch diameter Fig. 4a–c. A similar procedure was followed, and the % of a gap left in cells that were treated with $NiSO_4$, insulin, insulin + $NiSO_4$, were calculated and showed significant migration when compared to control. The cells treated with INiQCS + $Pb^{2+}$ show 44.24 ± 1.04%, 37.74 ± 2.93% and 27.42 ± 1.63% after 6, 12, and 24 h, respectively, as shown in Fig. 4u–w. Similarly, the migration after 6, 12, and 24 h comes out to be 49.69 ± 4.29%, 52.52 ± 7.28%, and 35.46 ± 0% in cells incubated with insulin + $NiSO_4$ as can be seen in Fig. 4j–l. In cells treated with insulin, the value of migration is 64.24 ± 4.66%, 63.42 ± 4.71% and 62.83 ± 11.46% after the time duration of 6, 12 and 24 h Fig. 4g–i while it is 82.72 ± 4.16%, 75.48 ± 4.85% and 71.63 ± 2.95% after the same time duration as above in cells treated with $NiSO_4$ as shown in Fig. 4d–f.

### 3.8. *In vitro* bio-imaging and sensing of $Pb^{2+}$

To confirm the wide applications of INiQCs for cellular imaging, bioimaging was performed on HEK293 cell lines. Cells were treated with INiQCs and show bright blue fluorescence due to the binding of INiQCs with the insulin receptors present on the cell wall of each cell, thus illuminating the cell walls and making cells look fluorescent. The imaging was performed on HEK 293 cell line after treating with INiQCs at both white and violet light, respectively, in the absence of a magnet Fig. 5a and b. The cells are showing bright blue-tinged fluorescence. Moreover, when the magnet was used while capturing the pictures, the fluorescence becomes much brighter, indicating the paramagnetic effect of $Ni^{2+}$ ions under white and violet light, respectively, Fig. 5c and d. This indicates the quantum

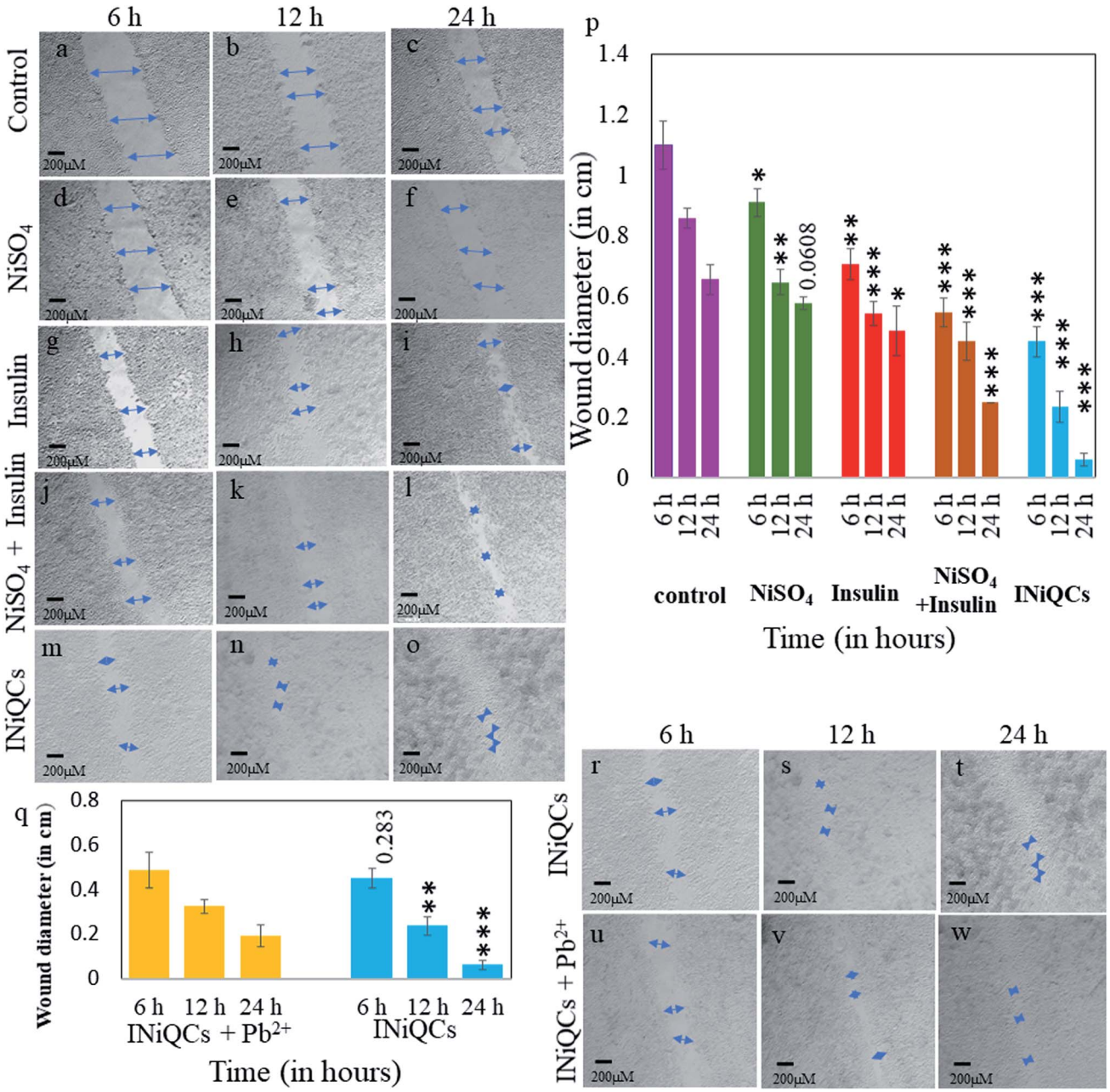


Fig. 4 Promotion and monitoring recovery of $Pb^{2+}$ poisoned wound using INiQCs *in vitro*. INiQCs induced better-wound recovery in comparison with only Ni salt or insulin or insulin + $NiSO_4$. HEK-293 cells control (a) 6 h, (b) 12 h, and (c) 24 h respectively and treated with 0.45 μM Ni salt for (d) 6 h, (e) 12 h, and (f) 24 h respectively, treated with insulin for (g) 6 h, (h) 12 h, and (i) 24 h respectively, treated with insulin + $NiSO_4$ (j) 6 h, (k) 12 h, and (l) 24 h respectively, treated with INiQCs for (m) 6 h, (n) 12 h, and (o) 24 h (p) plot shows the variation in wound diameter after 6 h, 12 h, 24 h post-treatment with Ni salt, insulin, insulin + $NiSO_4$ and INiQCs respectively. (q) Plot showing a comparison of the change in wound diameter post-treatment with INiQCs and INiQCs + $Pb^{2+}$ again 6 h, 12 h, 24 h post-treatment. The statistical significance of data is shown in both the plots with "*", ***$p < 0.001$, **$p < 0.01$, and *$p < 0.05$ respectively. Change in diameter of the wound is shown after its treatment with INiQCs for (r) 6 h, (s) 12 h, and (t) 24 h respectively and after its treatment with INiQCs + $Pb^{2+}$ for (u) 6 h, (v) 12 h and (w) 24 h respectively.

clusters emit bright fluorescence and, therefore, can be used for bioimaging purposes. The same experiment was performed in the presence of $Pb^{2+}$ ions. In this, the cells after treatment with INiQCs were treated with (0, 1, 10, 100, 500, 1000) μM $Pb^{2+}$ ions respectively and incubated. Thereafter, images were taken in white and violet light. It was observed that as we go on increasing the concentration of $Pb^{2+}$ ions, there was a gradual decline in fluorescence of cells that is fluorescence quenching occurs with increased concentration of heavy metal even up to 1 μM level indicating that even though the lead is toxic but still the INiQCs overcome its effect even at its highest concentrations and emit fluorescence thus can be used even in these conditions for bioimaging. The variation in fluorescence with

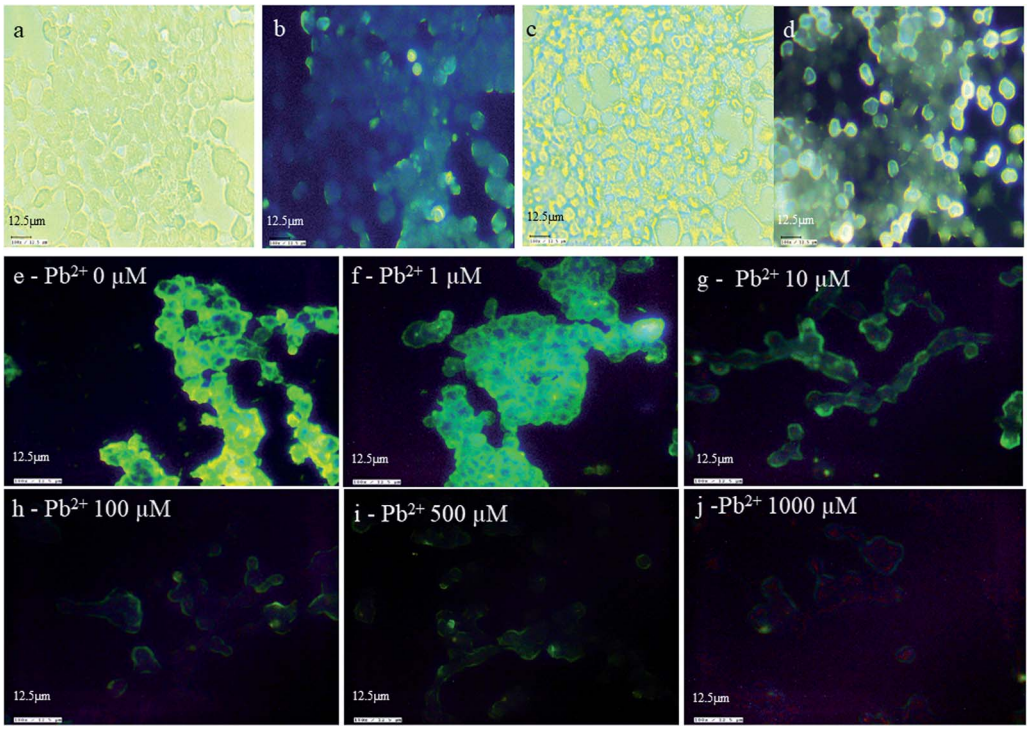


Fig. 5 *In vitro* imagining and HEK 293 cell line and sensing of $Pb^{2+}$ using INiQCs (a) in absence of magnet at the white light. (b) In the absence of a magnet at violet light (c) in the presence of a magnet at white light (d) in the presence of a magnet at violet light. Imaging of HEK 293 cell line on treatment with INiQCs (0.45 μM) followed by addition of different concentrations of $Pb^{2+}$ ions as (e) 0 μM $Pb^{2+}$, (f) 1 μM $Pb^{2+}$, (g) 10 μM $Pb^{2+}$, (h) 100 μM $Pb^{2+}$, (i) 500 μM $Pb^{2+}$, (j) 1000 μM $Pb^{2+}$ all under violet light respectively.

different concentrations of heavy metal ions (0, 1, 10, 100, 500, 1000) μM $Pb^{2+}$ is shown in Fig. 5e–j, respectively.

## 4. Conclusion

Lead-induced toxicity is very prevalent since earlier times. Although the overuse of lead is controlled in developed countries like Canada, USA and European Union but developing and underdeveloped countries are still excessively using it due to its certain physicochemical properties, which are of particular interest to humans. Lead affects all age groups, but infants are more prone to lead toxicity. Lead gets accumulated slowly in all the organs and causes inflammation. Diabetic patients are severely affected due to its accumulation leading to delay in wound recovery, thus needs to be taken care of efficiently. For this, we have prepared INiQCs, which contain an anti-inflammatory effect, and both nickel and insulin play a role in wound healing. These QCs were used to detect the heavy metal ion named $Pb^{2+}$ in a cell-free system and *in vitro* up to certain minimum levels of picomolar range and that too by using deficient concentrations of INiQCs in micromolar range thus preventing its highly toxic effects. Thereafter, INiQCs' effect on wound healing was checked both in the presence and absence of lead. Different techniques were used to confirm their formation, including TEM micrography, elemental analysis, FTIR, and metal ion binding site prediction and docking server (MIB) to confirm the interaction of Ni-metal with the insulin protein. From FTIR, we got peaks that show intermolecular interaction between Ni and insulin that is a peak at 670 $cm^{-1}$ and 820 $cm^{-1}$ showing Ni–OH bending and bond between Ni=O, respectively. The metal-ion binding site prediction and docking server were used for finding out the possible sites for the metal ion to bind with insulin amino acid chains A and B. In chain B, there was a binding site for $Ni^{2+}$ ions, and amino acids 9 SER and 10 HIS were used to form the groove. The binding potential was maximum for serine and histidine.

Moreover, INiQCs are target-specific quantum clusters. They exhibit the property of binding to insulin receptors present on the cells due to the use of insulin protein in their formation. This target-specific property of these particles makes them unique from other particles in various respects. First, these particles exhibit fluorescence (blue fluorescence) which easily distinguishes them from control insulin. Second, they have enhanced fluorescent properties, which can be easily detected using fluorescence microscopy. Third, in the presence of a magnet, their fluorescence enhanced manifolds compared to the one without using a magnet. Fourth, the INiQCs proved to be very specific for the particular lead metal ion indicating its high selectivity even in the presence of other interfering ions. This activity indicates its use as a fluorescence turn-off probe. It can be used in electronic and digital devices for several years for heavy metal detection. Thus, it has a wide range of applications in bio labeling and biosensing and material and biomaterial sciences and thus can be further explored for *in vivo* applications.

## Author contributions

Conceptualization: D. S., K. A., D. C.; methodology development: D. S., K. A., P. K.; data collection: D. S., K. A., P. K.; data analysis: D. S., K. A., P. K.; supervision: D. C.; visualization: D. S., K. A.; writing original draft: D. S.; writing – review & editing: D. S., P. K.; funding acquisition: D.C.

## Conflicts of interest

There are no conflicts to declare.

## Acknowledgements

DC is thankful to TIET-VT-CEEMS and SCBC for the instrumental facilities. K. A. is thankful to TIET-VT CEEMS for the fellowship. P.K. is thankful to DST, Govt. Of India, for a fellowship under the inspire scheme (award no. IF160636).

## References

1 E. Metryka, K. Chibowska, I. Gutowska, A. Falkowska, P. Kupnicka, K. Barczak, D. Chlubek and I. Baranowska-Bosiacka, Lead (Pb) Exposure Enhances Expression of Factors Associated with Inflammation, *Int. J. Mol. Sci.*, 2018, **19**(6), 1813.

2 F. Zhou, G. Yin, Y. Gao, D. Liu, J. Xie, L. Ouyang, Y. Fan, H. Yu, Z. Zha, K. Wang, L. Shao, C. Feng and G. Fan, Toxicity Assessment Due to Prenatal and Lactational Exposure to Lead, Cadmium and Mercury Mixtures, *Environ. Int.*, 2019, **133**, 105192.

3 N. Idrees, R. Sarah, B. Tabassum and E. F. Abd_Allah, Evaluation of some heavy metals toxicity in Channa punctatus and riverine water of Kosi in Rampur, Uttar Pradesh, India, *Saudi J. Biol. Sci.*, 2020, **27**, 1191–1194.

4 S. Madhavan, K. D. Rosenman and T. Shehata, Lead in Soil: Recommended Maximum Permissible Levels, *Environ. Res.*, 1989, **49**, 136–142.

5 M. Kumar and A. Puri, A Review of Permissible Limits of Drinking Water, *Indian J. Occup. Environ. Med.*, 2012, **16**, 40–44.

6 M. E. Abd El-Hack, S. A. Abdelnour, A. E. M. E. Abd El-Moneim, M. Arif, A. Khafaga, H. Shaheen, D. Samak and A. A. Swelum, Putative Impacts of Phytogenic Additives to Ameliorate Lead Toxicity in Animal Feed, *Environ. Sci. Pollut. Res.*, 2019, **26**, 23209–23218.

7 G. Wang, J. Tang, Q. Song, Q. Yu, C. Yao, P. Li, Y. Ding, M. Lin and D. Cheng, Malus Micromalus Makino Phenolic Extract Preserves Hepatorenal Function by Regulating PKC-A Signaling Pathway and Attenuating Endoplasmic Reticulum Stress in Lead(II) Exposure Mice, *J. Inorg. Biochem.*, 2020, **203**, 110925.

8 A. Soussi, M. Gargouri, A. Akrouti and A. El Feki, Antioxidant and Nephro-Protective Effect of Juglans Regia Vegetable Oil Against Lead-Induced Nephrotoxicity in Rats and Its Characterization by GC-MS, *EXCLI J.*, 2018, **17**, 492–504.

9 R. B. Jain, Co-exposures to Toxic Metals Cadmium, Lead, and Mercury and Their Impact on Unhealthy Kidney Function, *Environ. Sci. Pollut. Res.*, 2019, **26**, 30112–30118.

10 J. J. Carmouche, J. E. Puzas, X. Zhang, P. Tiyapatanaputi, D. A. Cory-Slechta, R. Gelein, M. Zuscik, R. N. Rosier, B. F. Boyce, R. J. O'Keefe and E. M. Schwarz, Lead Exposure Inhibits Fracture Healing and is Associated with Increased Chondrogenesis, Delay in Cartilage Mineralization, and a Decrease in Osteoprogenitor Frequency, *Environ. Health Perspect.*, 2005, **113**, 749–755.

11 M. S. de Oliveira, W. A. da Costa, D. S. Pereira, J. R. S. Botelho, T. O. de Alencar Menezes, E. H. de Aguiar Andrade, S. H. M. da Silva, A. P. da Silva Sousa Filho and R. N. de Carvalho, Chemical Composition and Phytotoxic Activity of Clove (Syzygium aromaticum) Essential Oil Obtained with Supercritical $CO_2$, *J. Supercrit. Fluids*, 2016, **118**, 185–193.

12 L. Struzyńska, B. Dąbrowska-Bouta, K. Koza and G. Sulkowski, Inflammation-Like Glial Response in Lead-Exposed Immature Rat Brain, *Toxicol. Sci.*, 2007, **95**, 156–162.

13 R. L. Ruebner, S. R. Hooper, C. Parrish, S. L. Furth and J. J. Fadrowski, Environmental Lead Exposure is Associated with Neurocognitive Dysfunction in Children with Chronic Kidney Disease, *Pediatr. Nephrol.*, 2019, **34**, 2371–2379.

14 G. Azeh Engwa, P. Udoka Ferdinand, F. Nweke Nwalo and M. N. Unachukwu, *Poisoning in the Modern World: New Tricks for an Old Dog?*, IntechOpen, 2019.

15 B. Kaličanin and D. Velimirović, A Study of the Possible Harmful Effects of Cosmetic Beauty Products on Human Health, *Biol. Trace Elem. Res.*, 2016, **170**, 476–484.

16 T. L. Pan, P. W. Wang, S. A. Al-Suwayeh, C. C. Chen and J. Y. Fang, Skin Toxicology of Lead Species Evaluated by Their Permeability and Proteomic Profiles: a Comparison of Organic and Inorganic Lead, *Toxicol. Lett.*, 2010, **197**, 19–28.

17 P. Zhu, J. Hawkins, W. H. Linthicum, M. Wang, N. Li, N. Zhou, Q. Wen, A. Timme-Laragy, X. Song and Y. Sun, Heavy Metal Exposure Leads to Rapid Changes in Cellular Biophysical Properties, *ACS Biomater. Sci. Eng.*, 2020, **6**, 1965–1976.

18 S. Pérez-Debén, R. Gonzalez-Martin, A. Palomar, A. Quiñonero, S. Salsano and F. Dominguez, Copper and Lead Exposures Disturb Reproductive Features of Primary Endometrial Stromal and Epithelial Cells, *Reprod. Toxicol.*, 2020, **93**, 106–117.

19 Y. Fujiwara, T. Kaji, S. Sakurai, M. Sakamoto and H. Kozuka, Inhibitory Effect of Lead on the Repair of Wounded Monolayers of Cultured Vascular Endothelial Cells, *Toxicology*, 1997, **117**, 193–198.

20 L. Tutkun, M. Gunduzoz, O. Oztan, V. Ali Turksoy, M. Erdem Alaguney and S. Birgin Iritas, The Relation Between Lead Exposure and Inflammation/Endothelial Dysfunction, *Med. Sci.*, 2020, **9**(2), 468–472.

21 M. Boskabady, N. Marefati, T. Farkhondeh, F. Shakeri, A. Farshbaf and M. H. Boskabady, The Effect of Environmental Lead Exposure on Human Health and the

Contribution of Inflammatory Mechanisms, a Review, *Environ. Int.*, 2018, **120**, 404–420.

22 N. Goswami, A. Giri, M. S. Bootharaju, P. L. Xavier, T. Pradeep and S. K. Pal, Copper Quantum Clusters in Protein Matrix: Potential Sensor of $Pb^{2+}$ Ion, *Anal. Chem.*, 2011, **83**, 9676–9680.

23 B. Das, D. Bodhisatwa and C. P. Sharma, Heavy Metal Sensing by Protein Stabilized Gold Quantum Clusters: A Quantitative Approach, *Trends Biomater. Artif. Organs*, 2012, **26**(3), 130–138.

24 V. D'Antò, R. Valletta, M. Amato, H. Schweikl, M. Simeone, S. Paduano, S. Rengo and G. Spagnuolo, Effect of Nickel Chloride on Cell Proliferation, *Open Dent. J.*, 2012, **6**, 177–181.

25 G. I. Stangl and M. Kirchgessner, Nickel Deficiency Alters Liver Lipid Metabolism in Rats, *J. Nutr.*, 1996, **126**, 2466–2473.

26 J. Ding, G. He, W. Gong, W. Wen, W. Sun, B. Ning, S. Huang, K. Wu, C. Huang, M. Wu, W. Xie and H. Wang, Effects of Nickel on Cyclin Expression, Cell Cycle Progression and Cell Proliferation in Human Pulmonary Cells, *Cancer Epidemiol., Biomarkers Prev.*, 2009, **18**(6), 1720–1729.

27 F. Wang, W. B. Tan, Y. Zhang, X. Fan and M. Wang, Luminescent Nanomaterials for Biological Labelling, *Nanotechnology*, 2006, **17**, R1–R13.

28 C. Li, W. Chen, D. Wu, D. Quan, Z. Zhou, J. Hao, J. Qin, Y. Li, Z. He and K. Wang, Large Stokes Shift and High Efficiency Luminescent Solar Concentrator Incorporated with $CuInS_2$/ZnS Quantum Dots, *Sci. Rep.*, 2016, **5**, 17777.

29 Y. J. Jin, D. Araki, M. Teraguchi, T. Aoki and G. Kwak, Dimesitylboryl-Containing Polydiphenylacetylene with a Large Stokes Shift, High Fluorescence Efficiency, and Fluoride Ion Sensing Ability, *Polymer*, 2018, **148**, 310–315.

30 J. Zheng, P. R. Nicovich and R. M. Dickson, Highly Fluorescent Noble-Metal Quantum Dots, *Annu. Rev. Phys. Chem.*, 2007, **58**, 409–431.

31 H. Cha, J. H. Yoon and S. Yoon, Probing Quantum Plasmon Coupling Using Gold Nanoparticle Dimers with Tunable Interparticle Distances Down to the Subnanometer Range, *ACS Nano*, 2014, **8**, 8554–8563.

32 M. A. Habeeb Muhammed, S. Ramesh, S. S. Sinha, S. K. Pal and T. Pradeep, Two Distinct Fluorescent Quantum Clusters of Gold Starting from Metallic Nanoparticles by pH-Dependent Ligand Etching, *Nano Res.*, 2008, **1**, 333–340.

33 X. Le Guevel, Recent Advances on the Synthesis of Metal Quantum Nanoclusters and Their Application for Bioimaging, *IEEE J. Sel. Top. Quantum Electron.*, 2014, **20**(3), 45–56.

34 P. Kaur and D. Choudhury, Insulin Promotes Wound Healing by Inactivating NFkβP50/P65 and Activating Protein and Lipid Biosynthesis and alternating Pro/Anti-inflammatory Cytokines Dynamics, *Biomol. Concepts*, 2019, **10**, 11–24.

35 A. T. Lusk and G. K. Jennings, Characterization of Self-Assembled Monolayers Formed from Sodium *S*-Alkyl Thiosulfates on Copper, *Langmuir*, 2001, **17**(25), 7830–7836.

36 P. L. Xavier, K. Chaudhari, P. K. Verma, S. K. Pal and T. Pradeep, Luminescent Quantum Clusters of Gold in Transferrin Family Protein, Lactoferrin Exhibiting FRET, *Nanoscale*, 2010, **2**, 2769–2776.

37 N. Goswami, A. Baksi, A. Giri, P. L. Xavier, G. Basu, T. Pradeep and S. K. Pal, Luminescent Iron Clusters in Solution, *Nanoscale*, 2014, **6**, 1848–1854.

38 J. M. Liu, L. P. Lin, X. X. Wang, S. Q. Lin, W. L. Cai, L. H. Zhang and Z. Y. Zheng, Highly Selective and Sensitive Detection of $Cu^{2+}$ with Lysine Enhancing Bovine Serum Albumin Modified-Carbon Dots Fluorescent Probe, *Analyst*, 2012, **137**(11), 2637–2642.

39 R. Mehta, P. Kaur, D. Choudhury, K. Paul and V. Luxami, $Al^{3+}$ Induced Hydrolysis of Rhodamine-based Schiff-Base: Applications in Cell Imaging and Ensemble as CN Sensor in 100% Aqueous Medium, *J. Photochem. Photobiol., A*, 2019, **380**, 111851.

40 K. Chaudhari and T. Pradeep, Initial Growth Kinetics of Luminescent Quantum Clusters of Silver within Albumin Family Protein Templates, *J. Phys. Chem. C*, 2015, **119**, 9988–9994.

41 V. Poderys, M. Matulionytė-Safinė, D. Rupšys and R. Rotomskis, Protein Stabilized Au Nanoclusters: Spectral Properties and Photostability, *Lith. J. Phys.*, 2016, **56**, 55–65.

42 V. F. Razumov and S. A. Tovstun, Features of Luminescence of Colloidal Quantum Dot Clusters, *High Energy Chem.*, 2015, **49**, 44–47.

43 N. Roohani, R. Hurrell, R. Kelishadi and R. Schulin, Zinc and its Importance for Human Health: An Integrative Review, *J. Res. Med. Sci.*, 2013, **18**(2), 144–157.

44 M. Watanabe, H. Hayasaki, T. Tamayama and M. Shimada, Histologic Distribution of Insulin and Glucagon Receptors, *Braz. J. Med. Biol. Res.*, 1998, **31**(2), 243–256.

45 V. Papa, V. Pezzino, A. Costantino, A. Belfiore, D. Giuffrida, L. Frittitta, G. B. Vannelli, R. Brand, I. D. Goldfine and R. Vigneri, Elevated Insulin Receptor Content in Human Breast Cancer, *J. Clin. Invest.*, 1990, **86**(5), 1503–1510.

46 A. Oryan and E. Alemzadeh, Effects of Insulin on Wound Healing: A Review of Animal and Human Evidences, *Life Sci.*, 2017, **174**, 59–67.

47 P. Kaur, A. K. Sharma, D. Nag, A. Das, S. Datta, A. Ganguli, V. Goel, S. Rajput, G. Chakrabarti, B. Basu and D. Choudhury, Novel Nano-Insulin Formulation Modulates Cytokine Secretion and Remodeling to Accelerate Diabetic Wound Healing, *Nanomed. Nanotechnol. Biol. Med.*, 2019, **15**(1), 47–57.

48 P.-F. Chen, C.-L. Liu, W.-K. Lin, K.-C. Chen, P.-T. Chou and S.-W. Chu, Fluorescence Depletion Properties of Insulin-Gold Nanoclusters, *Biomed. Opt. Express*, 2015, **6**(8), 3066.

49 P. Kaur, S. Sharma, S. D. Choudhury, D. Singh, S. Sharma, K. Gadhave, N. Garg and D. Choudhury, Insulin-Copper Quantum Clusters Preparation and Receptor Targeted Bioimaging, *Colloids Surf., B*, 2020, **188**, 110785.

50 J. Xie, Y. Zheng and J. Y. Ying, Protein-Directed Synthesis of Highly Fluorescent Gold Nanoclusters, *J. Am. Chem. Soc.*, 2009, **131**(3), 888–889.

51 J. Lin, Z. Zhou, Z. Li, C. Zhang, X. Wang, K. Wang, G. Gao, P. Huang and D. Cui, Biomimetic One-Pot Synthesis of Gold Nanoclusters/Nanoparticles for Targeted Tumor Cellular Dual-Modality Imaging, *Nanoscale Res. Lett.*, 2013, **8**(1), 1–7.

52 C.-L. Liu, H.-T. Wu, Y.-H. Hsiao, C.-W. Lai, C.-W. Shih, Y.-K. Peng, K.-C. Tang, H.-W. Chang, Y.-C. Chien, J.-K. Hsiao, J.-T. Cheng and P.-T. Chou, Insulin-Directed Synthesis of Fluorescent Gold Nanoclusters: Preservation of Insulin Bioactivity and Versatility in Cell Imaging, *Angew. Chem., Int. Ed.*, 2011, **50**, 7056–7060.

53 A. G. Murzin, S. E. Brenner, T. Hubbard and C. Chothia, SCOP: a Structural Classification of Proteins Database for the Investigation of Sequences and Structures, *J. Mol. Biol.*, 1995, **247**, 536–540.

54 G. Monnier, E. Frahm, B. Luo and K. Missal, Developing FTIR Microspectroscopy for Analysis of Plant Residues on Stone Tools, *J. Archaeol. Sci.*, 2017, **78**, 158–178.

55 C.-H. Lu, Y.-F. Lin, J.-J. Lin and C.-S. Yu, Prediction of Metal Ion–Binding Sites in Proteins Using the Fragment Transformation Method, *PLoS One*, 2012, **7**, e39252.

56 J. C. Gower and G. J. S. Ross, Minimum Spanning Trees and Single Linkage Cluster Analysis, *J. Appl. Stat.*, 1969, **18**, 54.

57 C.-H. Lu, Y.-S. Lin, Y.-C. Chen, C.-S. Yu, S.-Y. Chang and J.-K. Hwang, The Fragment Transformation Method to Detect the Protein Structural Motifs, *Proteins: Struct., Funct., Bioinf.*, 2006, **63**, 636–643.

58 Y. Shi, C. Tian, X. Yu, Y. Fang, X. Zhao, X. Zhang and D. Xia, Protective Effects of *Smilax glabra* Roxb. Against Lead-Induced Renal Oxidative Stress, Inflammation and Apoptosis in Weaning Rats and HEK-293 Cells, *Front. Pharmacol.*, 2020, **11**, 556248.

59 J. Li, M. Wei, W. Chu and N. Wang, High-Stable α-Phase NiCo Double Hydroxide Microspheres via Microwave Synthesis for Supercapacitor Electrode Materials, *Chem. Eng. J.*, 2017, **316**, 277–287.

60 H. Qiao, Z. Wei, H. Yang, L. Zhu and X. Yan, Preparation and Characterization of NiO Nanoparticles by Anodic Arc Plasma Method, *J. Nanomater.*, 2009, **2009**, 795928.

61 S. Bhakya, S. Muthukrishnan, M. Sukumaran and M. Muthukumar, Biogenic Synthesis of Silver Nanoparticles and Their Antioxidant and Antibacterial Activity, *Appl. Nanosci.*, 2016, **6**, 755–766.

62 B. De Campos Vidal and M. L. S. Mello, Collagen Type I Amide I Band Infrared Spectroscopy, *Micron*, 2011, **42**(3), 283–289.

63 A. Mitsuzuka, A. Fujii, T. Ebata and N. Mikami, Infrared Spectroscopy of Intramolecular Hydrogen-Bonded OH Stretching Vibrations in Jet-Cooled Methyl Salicylate and Its Clusters, *J. Phys. Chem. A*, 1998, **102**(48), 9779–9784.